JOURNAL OF CATALYSIS 134, 24–35 (1992)

Investigation of Synergy Effects in Selective Oxidation Catalysts through *in Situ* Laser Raman Spectroscopy/Isotopic Labeling Technique

UMIT S. OZKAN,[1] MARIANNE R. SMITH, AND SHARON A. DRISCOLL

Department of Chemical Engineering, The Ohio State University, Columbus, Ohio 43210

Received April 5, 1991; revised September 27, 1991

Previous studies over two-phase catalysts consisting of a simple molybdate ($MnMoO_4$, $CdMoO_4$) in close contact with molybdenum oxide (MoO_3) have shown the existence of a strong synergy effect in partial oxidation of C_4 hydrocarbons to maleic anhydride. In this paper, we present results of the investigation of this synergy effect using an isotopic labeling technique coupled with *in situ* laser Raman spectroscopy. Results from these studies, when integrated with our previous work, provide complementary evidence for the catalytic job distribution of the two phases, in which the MoO_3 phase incorporates its lattice oxygen into the hydrocarbon molecule, while the simple molybdate phase provides the oxygen necessary to regenerate MoO_3 sites through an oxygen spillover mechanism. The *in situ* Raman spectroscopy experiments combined with structural specificity studies provide further clues about the catalytic sites responsible for selective versus complete oxidation.

INTRODUCTION

Selective oxidation reactions are involved in the formation of a large number of intermediates and products which are important industrial chemicals, including many alcohols, aldehydes, ketones, and acids. The most effective industrial selective oxidation catalysts are generally multicomponent metal oxides that have catalytic properties pronouncedly different from those of the individual components. While the overall performance of a partial oxidation catalyst can be well documented, there are still gaps in the fundamental understanding of many of the steps involved in the reaction scheme and the oxygen insertion mechanism. The catalytic job distributions are often complex, involving many steps and multiple sites in the reaction scheme. Studies on model catalysts often prove useful in gaining insight into the phenomena affecting the performance of more complex catalytic systems.

One important application of selective oxidation catalysis is found in the production of maleic anhydride, which is an important intermediate for the polymer industry. The feedstock for this process has recently been changed to C_4 hydrocarbons, partly due to tighter emission controls for benzene, the original feedstock. Studies have shown vanadium–phosphorus–oxide (V–P–O) (*1–5*) as well as molybdate and molybdenum oxide (*6–16*) catalysts to be selective for the formation of maleic anhydride from C_4 hydrocarbons. The oxidation of 1-butene to maleic anhydride has been shown to proceed via the formation of an intermediate oxidative dehydrogenation product, 1,3-butadiene, and an intermediate partial oxidation product, furan, with complete oxidation appearing as a side reaction from each of the intermediate steps.

In our previous work, we reported a strong synergy effect between molybdenum oxide and a simple molybdate phase in two-phase catalysts ($MnMoO_4/MoO_3$, $CdMoO_4/MoO_3$) used for the formation of maleic anhydride (*13–16*). Transient and steady-state

[1] To whom correspondence should be addressed.

0021-9517/92 $3.00

reaction studies found the two-phase catalyst to be more selective than either pure phase. The two pure phases were found to have markedly different responses to the presence or absence of gas phase oxygen and its concentration, with $MnMoO_4$ showing a much stronger dependency on the concentration of gas phase oxygen.

When the synergy effect was further investigated through transient isotopic labeling techniques using $^{18}O_2$ for the gas phase oxygen (*17*), these studies also showed the source of oxygen for partial oxidation reactions over MoO_3 to be the catalyst lattice, while $MnMoO_4$ was found to utilize much more of the isotopic oxygen introduced through the feed gas. Based on the combined evidence, a catalytic job distribution was postulated to explain the synergy observed for the two-phase catalyst. The source of oxygen for selective oxidation reactions was said to be the lattice of the MoO_3 phase, while the $MnMoO_4$ phase contained sites that chemisorbed gas phase oxygen and allowed it to migrate, possibly in an activated form, to the reduced sites on MoO_3 to regenerate them. A similar spillover mechanism has been postulated for other multiphase catalysts used for selective oxidation reactions forming acrolein from propylene and methacrolein from isobutene (*18–20*).

Our more recent studies have focused on using isotopic labeling in conjunction with *in situ* laser Raman spectroscopy to shed further light on the nature of active sites and the oxygen insertion process. This technique has been successfully used to investigate other selective oxidation catalytic systems (*21–23*). Glaeser *et al.* (*21*) have used different hydrocarbon molecules over bismuth molybdate catalysts as probes to distinguish the α-hydrogen abstraction sites from those used for selective oxidation. Matsuura *et al.* (22) also used the combined techniques of isotopic labeling and Raman spectroscopy to identify the sites that take part in lattice oxygen insertion over bismuth molybdate catalysts in propylene oxidation. Another successful application of this technique has been reported by Schrader and co-workers (*23*) in a study of V–P–O catalysts for the production of maleic anhydride. In this study, the isotopically labeled oxygen atoms were first incorporated into specific lattice sites, and the isotopic distribution of the product stream and the Raman band shifts were followed as reduction of the catalyst with *n*-butane and 1-butene progressed.

For the work presented in this paper, the active oxidation sites in MoO_3, $MnMoO_4$, and the two-phase catalyst $MnMoO_4/MoO_3$ were investigated using isotopic labeling in conjunction with *in situ* Raman spectroscopy. Catalyst samples that were reduced by 1,3-butadiene were reoxidized using $^{18}O_2$ in the gas phase, thus allowing observation of the Raman band shifts due to the isotope effect. These observations, combined with our previous work focusing on structural specificity of MoO_3 (*24*), provide further insight into the catalytic job distribution and the mechanism of synergy in these model multicomponent catalysts for selective oxidation reactions.

EXPERIMENTAL METHODS

Catalyst preparation and characterization. The MoO_3 used in the *in situ* Raman spectroscopy experiments was obtained from Aldrich and was used as supplied. $MnMoO_4$ was prepared by precipitation from aqueous solutions of manganese chloride (J. T. Baker, $MnCl_2 \cdot 4H_2O$) and ammonium heptamolybdate (Fisher, $(NH_4)_6Mo_7O_{24} \cdot 4H_2O$). The two-phase catalyst was prepared via a stepwise "wet impregnation" technique, in which molybdenum trioxide samples were soaked in an aqueous suspension of manganese molybdate (*13*). The molybdenum trioxide samples used for structural specificity investigations were prepared by temperature-programmed thermal treatment techniques described previously (*24*). All three catalyst types were characterized by BET surface area, high-temperature oxygen chemisorp-

tion, X-ray diffraction, scanning electron microscopy, energy dispersive X-ray analysis, laser Raman spectroscopy, Raman microprobe, and X-ray photoelectron spectroscopy techniques. These methods have been described previously (*13, 17*). Scanning electron microscopy was also coupled with three-dimensional imaging techniques. The three-dimensional images were then digitized on a VAX 8550, and used to calculate accurate crystallographic plane ratios. This technique was also described in an earlier publication (*24*).

In situ Raman spectroscopy/isotopic labeling. Raman spectroscopy was combined with an isotopic labeling technique using an *in situ* cell with a Spex Ramalog-9-I spectrometer. An argon ion laser (Spectra Physics, 2016) was used as the excitation source. A quartz cell with optically clear windows was used to hold the catalyst sample. A specially designed stage held the *in situ* cell, and allowed for adjustments in the *x, y,* and *z* directions. Additionally, adjustments could be made in the tilting angle of the cell to achieve the optimum position of the cell relative to the incident radiation and the collection optics. The stage could also be raised to reaction temperature using resistive heating cartridges. A diagram of the system used in these studies is shown in Fig. 1. Each sample was loaded into the cell and raised to 450°C under a He flow of 8 sccm at 10 psig. A Raman spectrum was obtained at this temperature as a "base" scan. Catalyst samples at 450°C were then reduced for 1 h under a 10 sccm stream of 5% 1,3-butadiene in N_2 mixture at 10 psig. A spectrum was then accumulated under flowing He. The sample was reduced for another 1 h under the mixture flow, and another spectrum was taken. The cell was then pressurized to 10 psig with a 25% $^{18}O_2/N_2$ mixture for 30 min. After obtaining a spectrum, the cell was flushed and repressurized with fresh isotopic mixture for three additional 30-min cycles. This was followed by flushing the cell with He, and a spectrum was accumulated under flowing He. Shifts resulting from the incorporation of $^{18}O_2$ into the catalyst lattice could then be observed when these spectra were compared to the "base" scan. To ensure that observed shifts were due to an isotopic effect, control experiments were performed using $^{16}O_2$ in place of the isotope.

Post-reaction characterization studies. Results from characterization of fresh catalyst samples were compared to post-reaction/*in situ* characterization of catalyst samples using BET surface area, X-ray diffraction, X-ray photoelectron spectroscopy, and laser Raman spectroscopy. BET surface area measurements and X-ray diffraction analyses were performed after catalyst samples were exposed to steady-state reaction conditions for at least 16 h. These techniques have been described previously (*13*). X-ray photoelectron spectra of catalyst samples were obtained using a Physical Electronics/Perkin Elmer (Model 550)ESCA/Auger spectrometer, operated at 15 kV, 20 mA. The X-ray source was MgK_α radiation (1253.6 eV). The binding energy for C 1*s* (284.6 eV) was used as a reference in these measurements. Post-reaction XPS characterization was performed without exposing the samples to atmosphere. The post-reaction Raman characterization experiments were performed *in situ,* using the controlled atmosphere Raman cell described in the preceding section.

RESULTS

Prior to reduction/reoxidation studies, some control experiments were performed to assess the effect of temperature on the spectra. All bands exhibit some broadening compared to spectra obtained at room temperature due to bulk oscillations. There also appears to be a 3–4 cm^{-1} shift to smaller frequencies at high temperature. Figure 2 shows a comparison of the spectra of MoO_3 obtained at room temperature before heating, at 450°C, and after being cooled down to 35°C. While the high-temperature spectrum shows band broadening and slight shifts, the spectrum obtained after the sample is cooled down shows that there are no apparent irre-

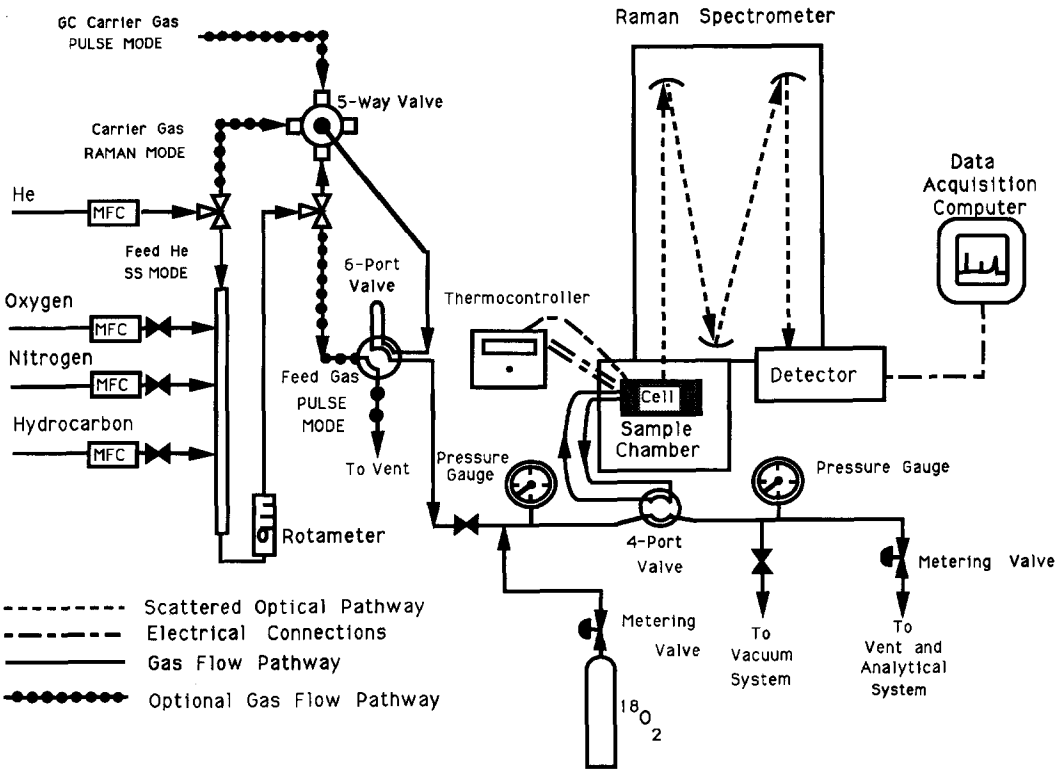

FIG. 1. *In situ* Raman spectroscopy system.

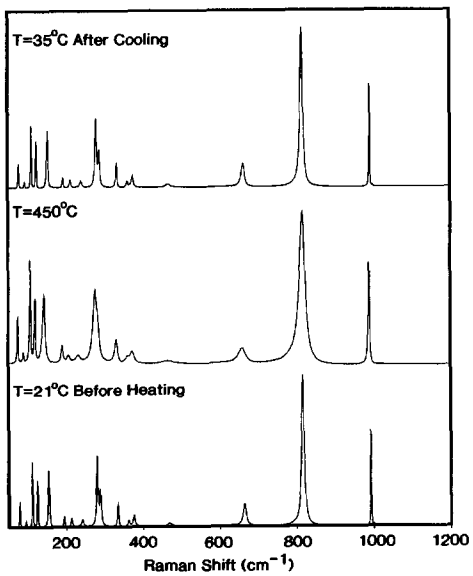

FIG. 2. Effect of heating on the laser Raman spectra of MoO_3.

versible changes that take place in the catalyst due to heating, since the spectrum reverts back to its original form when the sample is cooled down. The *in situ* Raman spectra of fresh and reduced samples are presented in Figs. 3, 4, and 5. All spectra were taken at 450°C in a controlled atmosphere. The reduction parameters were kept constant for all catalysts. The comparison of the spectra obtained over fresh and reduced MoO_3 (Fig. 3) shows a high degree of reduction as evidenced by the intensity loss of all the major Raman bands which are characteristic of this compound. Reduction of MoO_3 was also indicated by a color change of the sample from pale yellow to dark grey. Some of the intensity loss seen upon reduction may be attributed to this color change. The spectra obtained over $MnMoO_4$ exhibit some loss of intensity although the degree of reduction is not as severe as it is in MoO_3 (Fig. 4). The two-phase sample does not ap-

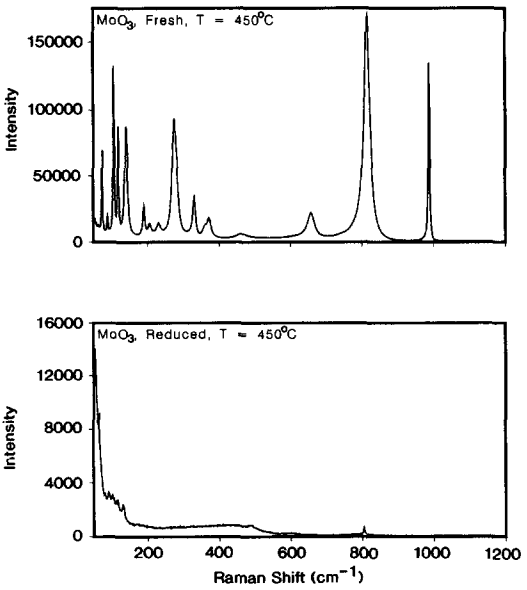

FIG. 3. Laser Raman spectra of fresh and reduced MoO_3.

pear to be reduced as much as pure MoO_3; however, when the relative intensities of the bands that correspond to MoO_3 and to $MnMoO_4$ are compared, one sees that the relative intensity loss of MoO_3 bands at 815 and 992 cm^{-1} is greater than the relative intensity loss of the $MnMoO_4$ bands at 926 and 860 cm^{-1} (Fig. 5).

XPS analyses were also performed over fresh samples and samples reduced under the same conditions as those used for *in situ* Raman runs. Reduced samples were transferred to the XPS chamber under an Ar atmosphere without being exposed to air. The binding energy values Mo $3d_{5/2}$ and Mo $3d_{3/2}$ did not show any major shifts due to reduction (Table 1). The half width values, however, showed considerable band broadening.

Figure 6 shows a comparison of the spectrum obtained from MoO_3 before reduction to that obtained after reduction with 1,3-butadiene and reoxidation with $^{18}O_2$. An examination of the two spectra presented in Fig. 6 shows very distinct shifts in the 815 and 991 cm^{-1} bands. An interesting feature about these shifts is the fact that the band at 815 cm^{-1} has been virtually replaced by a 789 cm^{-1} band. The band at 992 cm^{-1}, on the other hand, has split into two bands, one at 935 and one at the original position. Control experiments were performed to as-

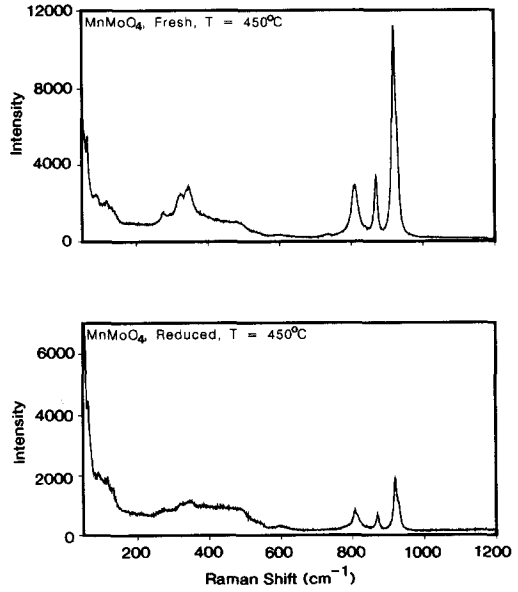

FIG. 4. Laser Raman spectra of fresh and reduced $MnMoO_4$.

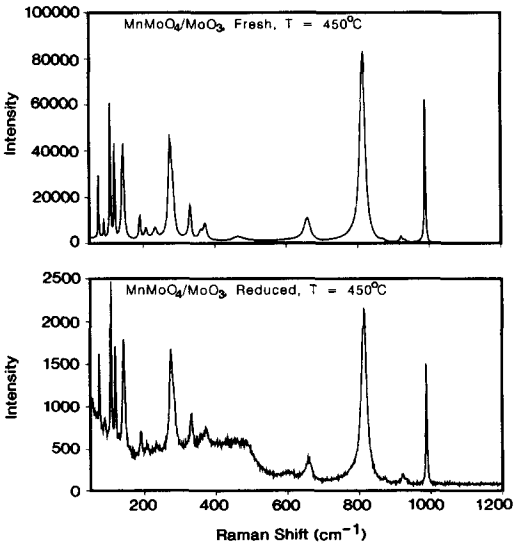

FIG. 5. Laser Raman spectra of fresh and reduced $MnMoO_4/MoO_3$.

TABLE 1

Binding Energy Values for Mo Obtained by X-Ray Photoelectron Spectroscopy

Sample	Mo($3d_{3/2}$) eV	Halfwidth	Mo($3d_{5/2}$) eV	Halfwidth
MoO_3 (fresh)	236.01	1.67	232.88	1.79
MoO_3 (reduced)	235.94	1.87	232.80	2.05

certain that the band shifts observed were indeed due to the isotope effect. Figure 7 shows spectra obtained from MoO_3 before reduction and after a reduction/reoxidation cycle using $^{16}O_2$. The second spectrum is almost identical to the spectrum obtained from the fresh catalyst. This type of control experiments provided proof that the shifts observed following reoxidation with $^{18}O_2$ were actually due to the isotope effect. Figure 8 shows the low wavenumber region of the two spectra obtained from MoO_3. In this region, the most pronounced shifts were the ones associated with the 231 and 331 cm^{-1} bands. After reoxidation with $^{18}O_2$, these bands have shifted to 225 and 322 cm^{-1}, respectively. The two spectra obtained over pure $MnMoO_4$ (Fig. 9), however, do not show any shifts due to isotope effect, exhibiting a markedly different behavior than the MoO_3 phase. The two-phase sample ($MnMoO_4/MoO_3$) shows a partial shift in MoO_3 bands, but no shift in the bands that correspond to $MnMoO_4$ (Fig. 10).

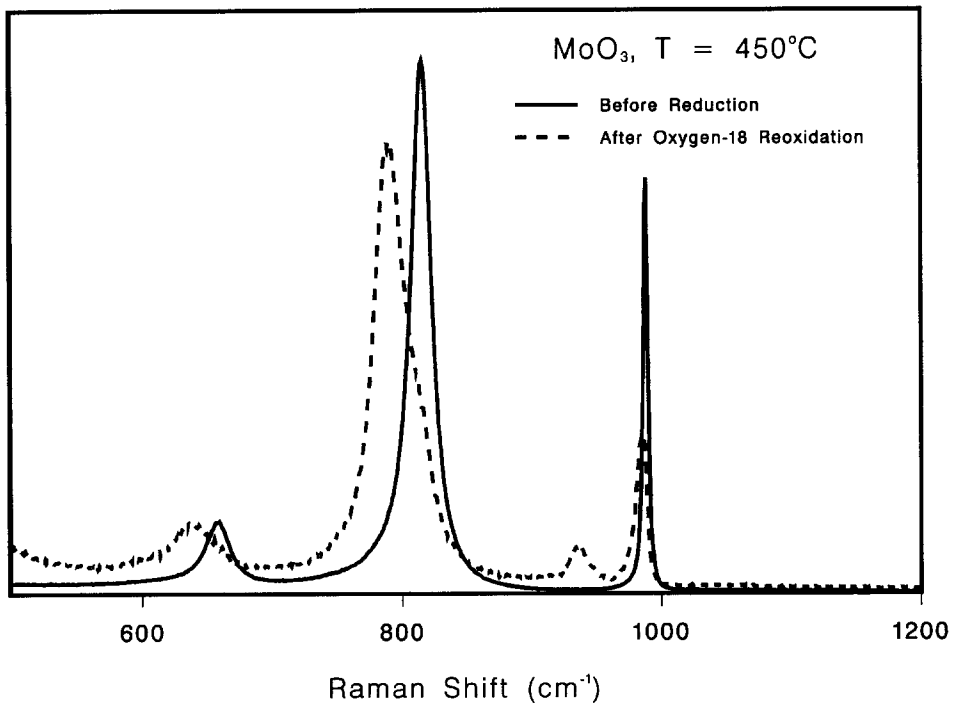

FIG. 6. Laser Raman spectra of MoO_3 before reduction and after reoxidation with $^{18}O_2$ (high wavenumber region).

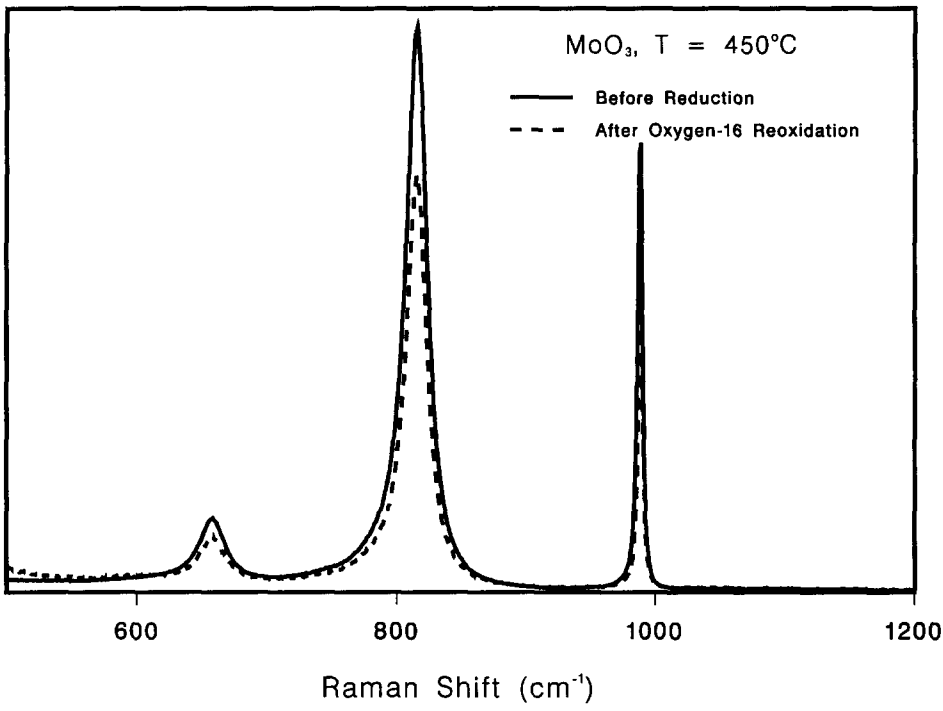

FIG. 7. Laser Raman spectra of MoO_3 before reduction and after reoxidation with $^{16}O_2$.

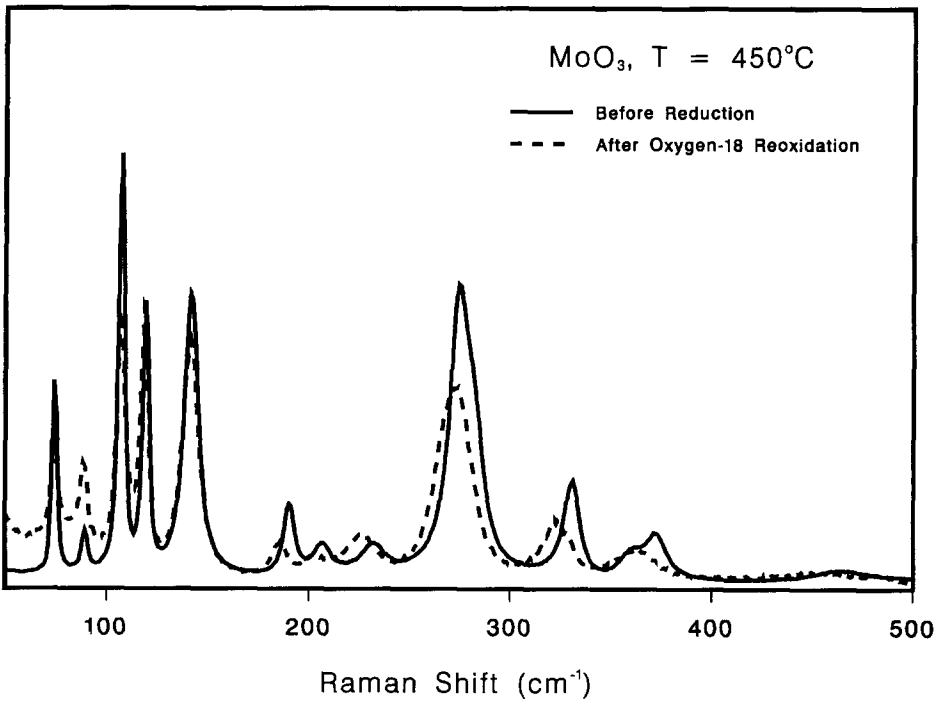

FIG. 8. Laser Raman spectra of MoO_3 before reduction and after reoxidation with $^{18}O_2$ (low wavenumber region).

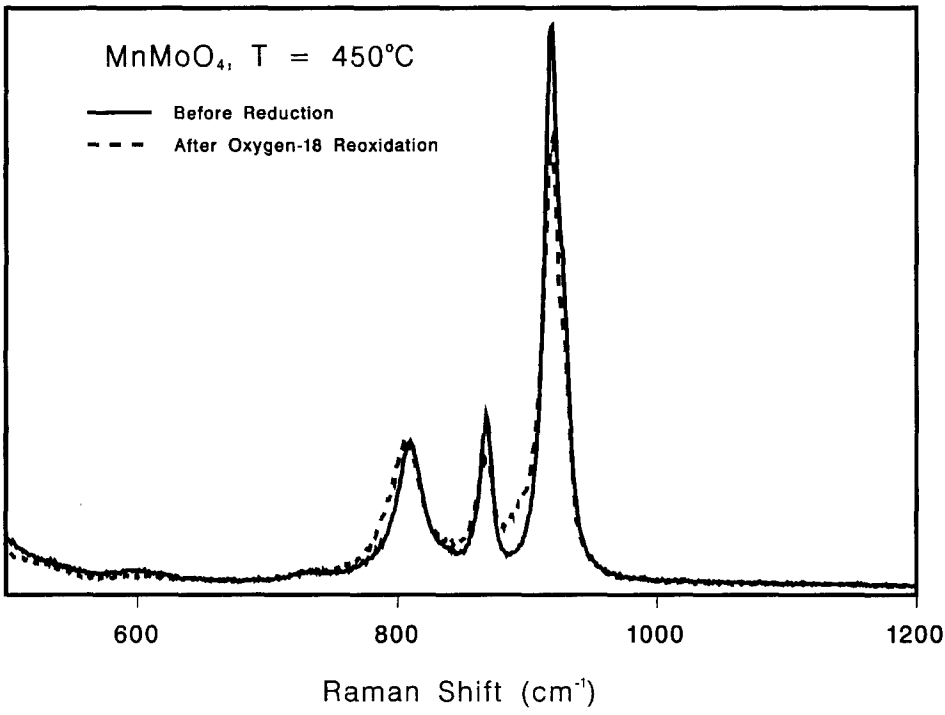

FIG. 9. Laser Raman spectra of $MnMoO_4$ before reduction and after reoxidation with $^{18}O_2$.

DISCUSSION

Initial studies that were performed over two-phase $MnMoO_4/MoO_3$ catalysts showed a strong synergy effect in the partial oxidation of C_4 hydrocarbons. Two-phase catalysts that brought a molybdenum oxide phase in close contact with a simple molybdate were observed to be much more active and selective for partial oxidation products than either of the pure phases (*13*). This behavior persisted through a large variation of reaction parameters such as catalyst composition, conversion level, temperature, and oxygen concentration (*25*). A detailed characterization of the two-phase catalyst did not show the formation of a new phase or compound, but revealed a close proximity of the two phases. Similar studies using another simple molybdate, $CdMoO_4$, as the second phase with MoO_3 showed similar synergy effects, suggesting that the role played by manganese molybdate was not unique to this component (*16*).

Our recent studies that involved post-reaction/*in situ* characterization experiments also verified the coexistence of the two phases under reaction conditions. While post-reaction X-ray photoelectron spectroscopy studies that were performed without exposing samples to the atmosphere did not show any changes in binding energy values for molybdenum and manganese, post-reaction X-ray diffraction showed that the crystal structure of the samples remained intact after being exposed to reaction conditions for an extended period of time. *In situ* laser Raman spectroscopy also showed the existence of the two phases under reaction conditions.

The results of our laser Raman spectroscopy/isotopic labeling studies on single-phase and two-phase oxidation catalysts provide new, complementary evidence for explaining some of the catalytic phenomena observed through our earlier studies, and offer important clues about active oxidation sites.

The ease with which the MoO_3 phase is

reduced, as evidenced by comparison of spectra of the reduced catalysts, reinforces the hypothesis that oxygen in the MoO_3 lattice is utilized more easily than that of $MnMoO_4$, while $MnMoO_4$ relies on gas phase oxygen. While the MoO_3 spectrum disappeared almost completely, the $MnMoO_4$ spectrum showed only partial intensity loss. The two-phase sample showed a preferential intensity loss of MoO_3 Raman bands relative to $MnMoO_4$ bands. Previous chemisorption studies (*17*) over fresh and reduced samples are in agreement with this finding. These studies showed that while $MnMoO_4$ was much more adsorbent towards oxygen in fresh form, the oxygen uptake of MoO_3 became much larger than that of $MnMoO_4$ after reduction. This change is due to the difference in the degree of reduction achieved over the two single-phase catalysts, with MoO_3 reducing more readily than $MnMoO_4$. Reaction studies (*15*) have also shown MoO_3 to be quite insensitive to changes in the gas phase oxygen concentration, while manganese molybdate showed a strong dependency on oxygen concentration, with its activity rapidly increasing with increasing oxygen concentration. Transient activity studies (*14*) over these catalysts in the absence and in the presence of gas phase oxygen have also shown that MoO_3 was able to utilize its lattice oxygen much more readily than $MnMoO_4$, while $MnMoO_4$ was more dependent on the presence of gas phase oxygen.

The spectra obtained from $MnMoO_4$ in fresh form and after reduction with 1,3-butadiene and reoxidation with $^{18}O_2$ were very similar, showing no detectable shifts in the band positions due to the isotope effect. The comparison of the spectra obtained from the fresh MoO_3 to those obtained after reduction/reoxidation with $^{18}O_2$, however, showed very distinct shifts, especially in the 815 and 991 cm^{-1} bands. An interesting feature about these shifts is that the 815 cm^{-1} band is completely replaced by the shifted band at 792 cm^{-1} whereas the band at 991 cm^{-1} is split into two distinct bands, one at 938 cm^{-1} and one at the original position. This observation is significant since the band at 815 cm^{-1} is associated with stretching vibration of the bridging oxygen bonds (Mo–O–Mo) and the band at 991 cm^{-1} is attributed to the Mo=O stretching vibrations (*26*). Since the major reaction product over MoO_3 in 1,3-butadiene oxidation is CO_2(*15*), this may suggest that the oxygen insertion that results in complete oxidation takes place on the Mo–O–Mo sites, although a secondary mechanism where adsorbed oxygen is used in CO_x formation may also be in operation. The band assignments in the low wavenumber region are not as straightforward as those in the high wavenumber region. However, using the band assignments reported by Beattie and Gilson (*26*), the bands which are associated with Mo–O–Mo deformation (190, 231, 331 cm^{-1}) are also seen to shift noticeably, while the bands associated with Mo=O deformations (274, 371 cm^{-1}) show a partial shift accompanied with some band broadening.

The spectrum obtained over the two-phase sample after reoxidation with $^{18}O_2$ shows similar shifts in MoO_3 bands while bands that correspond to $MnMoO_4$ remain in their original position. Transient isotopic labeling studies using $^{18}O_2$ in the gas phase (*17*) showed that over MoO_3, the oxygen incorporated into the partial oxidation products of 1,3-butadiene came almost exclusively from the lattice of MoO_3. The contribution of gas phase oxygen was much more significant over the $MnMoO_4$ phase. For total oxidation over MoO_3, the major source of oxygen was again the lattice; however, the contribution of the gas phase was also significant. Under the transient conditions of these experiments, $MnMoO_4/MoO_3$ was the only catalyst to yield substantial quantities of maleic anhydride, and results showed that nearly 90% of all oxygen incorporated into the hydrocarbon molecule to form maleic anhydride came from the crystal lattice of the catalyst, and the increase of the gas phase oxygen concentration was very slow.

A major difference between the spectra of

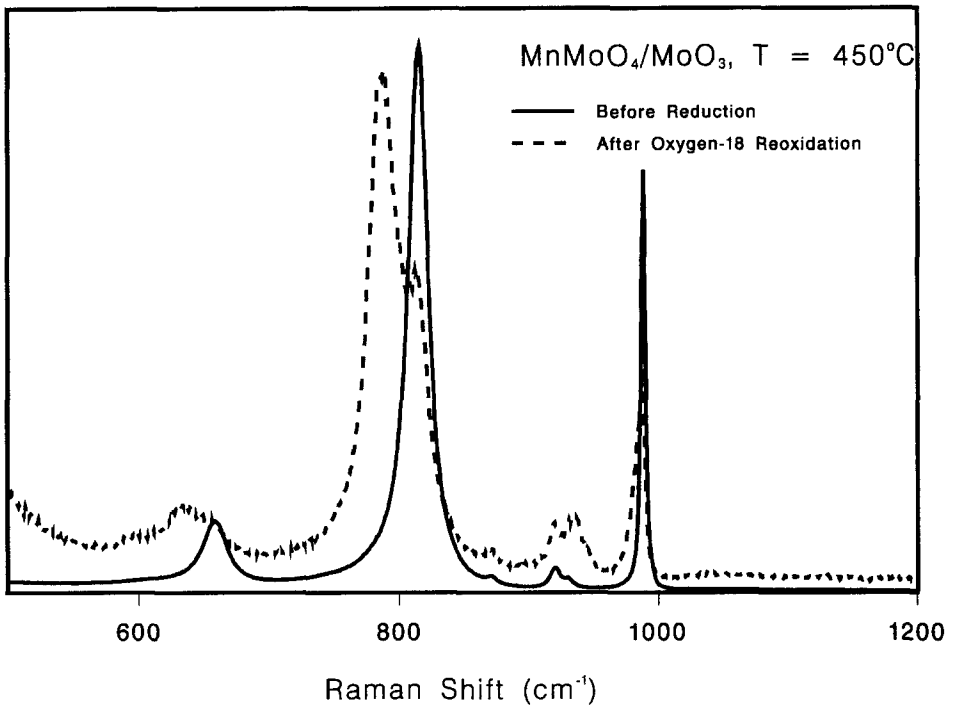

FIG. 10. Laser Raman spectra of $MnMoO_4/MoO_3$ before reduction and after reoxidation with $^{18}O_2$.

pure MoO_3 and the two-phase sample taken after reduction and reoxidation with $^{18}O_2$ is the fact that the 815 cm^{-1} band in the two-phase catalyst forms a shoulder band at 815 cm^{-1}, showing only a partial shift due to the isotope effect. This difference can be explained by the fact that the two-phase catalyst does not yield as much CO_2 as does pure MoO_3 (15).

Both previous reaction studies and our *in situ* laser Raman/isotopic labeling studies have shown a major difference in the way oxygen was utilized by the two components of the $MnMoO_4/MoO_3$ catalysts. The newer studies presented here support our previous suggestion of a catalytic job distribution between the two phases in which MoO_3 is responsible for introducing oxygen to the hydrocarbon from its lattice, forming the selective oxidation product. The role of the second phase (simple molybdate) involves chemisorption and possible activation of the gas phase oxygen and its transfer to the MoO_3 phase through an oxygen spillover process. The complete oxidation appears to take place on multiple sites over both of the phases, involving both lattice and gas phase oxygen.

Clues about the specific catalytic sites present on MoO_3 crystals are provided when earlier studies on the structural specificity of MoO_3 (*24*) are reexamined in light of the *in situ* Raman work. In the structural specificity studies, MoO_3 crystallites were grown with preferred orientation such that samples with varying basal-to-side area ratios (i.e., (010)/(100)) were obtained. Table 2 summarizes some of the catalytic activity measurements obtained over two MoO_3 samples that had distinctly different ratios of basal-to-side planes. A comparison of the product yields over the two samples showed that the MoO_3 samples with a higher ratio of basal-to-side plane area were more inclined to completely oxidize the hydrocarbon. This observation persisted for all three feed

TABLE 2

Comparison of Yields (μmol/min-m^2) over MoO_3 Catalysts with Different (010) to (100) Plane Ratios

	410°C		480°C		550°C		600°C	
	MoO_3-C	MoO_3-R	MoO_3-C	MoO_3-R	MoO_3-C	MoO_3-R	MoO_3-C	MoO_3-R
				1-Butene oxidation				
CO_2	2.64	5.54	21.0	28.4	68.3	111.0	131.0	255.0
C_4H_4O	0.132	0.00	1.11	0.835	5.94	5.86	4.49	4.08
$C_4H_2O_3$	0.725	0.659	6.49	3.71	28.3	20.4	26.6	13.4
				1,3-Butadiene oxidation				
CO_2	10.5	17.1	33.6	42.2	142.0	279.0	285.0	343.0
C_4H_4O	12.5	7.25	27.3	13.2	19.1	15.8	4.61	2.24
$C_4H_2O_3$	27.0	15.2	76.1	41.4	73.8	63.3	27.7	21.1
				Furan oxidation				
CO_2	38.6	36.6	370.0	456.0	687.0	795.0	1270.0	1390.0
$C_4H_2O_3$	155.0	77.1	592.0	198.0	390.0	216.0	106.0	58.8

stocks (1-butene, 1,3-butadiene, and furan) over the entire temperature range covered in this study (400 to 600°C). While the catalytic activity measurements exhibited a marked variation between the two samples, the laser Raman spectra of these samples also showed a pronounced difference in the relative intensities of the 815 and 991 cm^{-1} bands. As seen in Fig. 11, the intensity of the 815 cm^{-1} band was higher in the samples that gave a higher yield of complete oxidation products than it was in the MoO_3 samples that gave a lower selectivity towards CO and CO_2. This observation also points to the involvement of the Mo–O–Mo sites in the complete oxidation process. When samples with different side-to-plane ratios were examined *in situ* by Raman spectroscopy, this difference in intensity persisted.

In conclusion, the results from our previous investigations combined with our more recent studies give a better understanding of the catalytic phenomena involved in these multiphase catalysts. These results support the catalytic job distribution between the two phases in which the MoO_3 phase utilizes its lattice oxygen to form partial oxidation products. The role of the simple molybdate phase is to increase the rate at which reduced sites on the MoO_3 surfaces are regenerated by adsorbing the oxygen from the gas phase and allowing its migration to MoO_3 sites through an oxygen spillover mechanism. It is quite likely that this adsorption/migration step also involves activation of the oxygen species. While oxygen insertion that results in partial oxidation appears to be limited mostly to MoO_3 sites, there is probably more than one mechanism in operation that results in complete oxidation. Our results indicate that complete oxidation also utilizes oxygen from the lattice of the MoO_3 phase. However, it is quite likely that complete oxidation takes place through direct use of gas phase oxygen over MoO_3 surfaces as well as over the surfaces of the simple molybdate phase. Our *in situ* Raman spectroscopy/isotopic labeling studies and structural specificity investigations over MoO_3 crystallites suggest that Mo=O sites are involved in oxygen insertion steps that result in selective oxidation. Mo–O–Mo sites, on the other hand, appear to be involved in complete oxidation, although there are likely to be other concurrent mechanisms for the formation of CO_2 that involve use of adsorbed oxygen over both phases.

The *in situ* Raman spectroscopy technique coupled with isotopic labeling described herein has proven to be a valuable

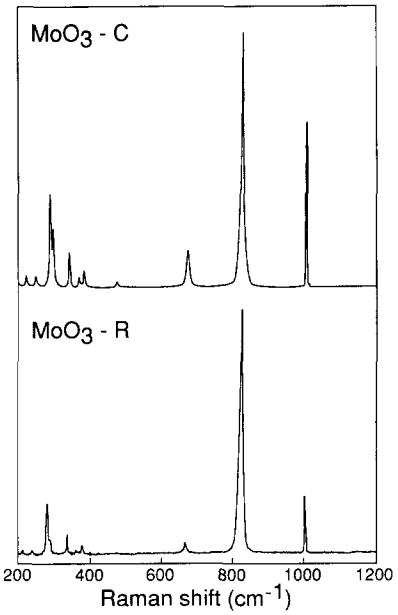

FIG. 11. Laser Raman spectra of MoO_3 crystals with different (010)/(100) plane ratios.

tool for investigating the catalytic job distribution of these model catalysts, and also for providing clues as to the identity of the active sites in these compounds when used as catalysts.

ACKNOWLEDGMENTS

Financial support from the ACS Petroleum Research Fund, from the AMAX Foundation, and from National Science Foundation through Grant CTS-8912247 is gratefully acknowledged.

REFERENCES

1. Ai, M., *Bull. Chem. Soc. Jpn.* **43,** 3490 (1970).
2. Ai, M., *Bull. Chem. Soc. Jpn.* **44,** 761 (1971).
3. Sunderland, P., *Ind. Eng. Chem. Prod. Res. Devel.* **15,** 90 (1976).
4. Cavani, F., Centi, G., Manenti, I., Riva, A., and Trifiro, F., *Ind. Eng. Chem. Prod. Res. Devel.* **22,** 565 (1983).
5. Centi, G., Fornasari, G., and Trifiro, F., *Ind. Eng. Chem. Prod. Res. Devel.* **24,** 32 (1985).
6. Trifiro, F., Caputo, G., and Villa, P. L., *J. Less-Common Met.* **36,** 305 (1974).
7. Trifiro, F., Caputo, G., and Forzatti, P., *Ind. Eng. Chem. Prod. Res. Devel.* **14**(1), 22 (1975).
8. Trifiro, F., Banfi, C., Caputo, G., Forzatti, P., and Pasquon, I., *J. Catal.* **30,** 393 (1973).
9. Ozkan, U. S., and Schrader, G. L., *J. Catal.* **95,** 120 (1985).
10. Ozkan, U. S., and Schrader, G. L., *J. Catal.* **95,** 137 (1985).
11. Ozkan, U. S., and Schrader, G. L., *J. Catal.* **95,** 147 (1985).
12. Ozkan, U. S., and Schrader, G. L., *Appl. Catal.* **23,** 327 (1986).
13. Ozkan, U. S., Gill, R. C., and Smith, M. R., *J. Catal.* **116,** 171 (1989).
14. Ozkan, U. S., Moctezuma, E., and Driscoll, S. A., *Appl. Catal.* **58,** 305 (1990).
15. Ozkan, U. S., Smith, M. R., and Driscoll, S. A., *J. Catal.* **123,** 173 (1990).
16. Ozkan, U. S., Gill, R. C., and Smith, M. R., *Appl. Catal.* **62,** 105 (1990).
17. Ozkan, U. S., Driscoll, S. A., Zhang, L., and Ault, K., *J. Catal.* **52,** 349 (1990).
18. Ruiz, P., Zhou, B., Remy, M., Machef, T., Aoun, F., Doumain, B., and Delmon, B., *Catal. Today* **1,** 181 (1987).
19. Weng, L. T., Ruiz, P., Delmon, B., and Duprez, D., *J. Mol. Catal.* **52,** 349 (1989).
20. Weng, L. T., Ma, S. Y., Ruiz, P., and Delmon, B., *J. Mol. Catal.* **61,** 99 (1990).
21. Glaeser, L., Brazdil, J., Hazle, M., Mehicic, M., and Grasselli, R., *J. Chem. Soc., Faraday Trans. 1* **79,** 2903 (1985).
22. Matsuura, I., Hashiba, H., and Kanesaka, I., *Chem. Lett.,* 533 (1986).
23. Lashier, M. E. and Schrader, G.L., *J. Catal.* **128,** 113 (1991).
24. Hernandez, R. A., and Ozkan, U. S., *Ind. Eng. Chem. Res.* **29**(7), 1454 (1990).
25. Gill, R. C., and Ozkan, U. S., *J. Catal.,* **122,** 452 (1990).
26. Beattie, I. R., and Gilson, T. R., *J. Chem. Soc. A,* 2322 (1969).